


Metamaterials with Reprogrammable Reciprocity

Austin Eichelberg, Audrey A. Watkins, and Osama R. Bilal^{✉*}
Department of Mechanical Engineering, University of Connecticut, Storrs, USA

 (Received 19 July 2022; revised 21 September 2022; accepted 27 September 2022; published 16 November 2022)

Metamaterials composed of asymmetric elements have been shown to break reciprocity; permitting the propagation of waves in one direction. The configuration of these metamaterials typically limits the propagation of the wave to a single direction, speed, or occurrence with little or no tunability. Here we present—theoretically, numerically, and experimentally—a simple design approach for reprogrammable metamaterials, which allows for all of these parameters to be tuned, enabled, disabled, or reset. We present a map of different geometries that allow for reciprocal and nonreciprocal wave propagation and attenuation. We show how a single design can be programmed on demand to support wave propagation and attenuation in both directions (reciprocal) or wave propagation in only one direction (nonreciprocal). In addition, we demonstrate real-time control of the wave velocity, both in amplitude and direction, as it propagates through the metamaterial. We show speeding up, slowing down, or complete reversal of the propagating wave direction. Furthermore, we show that the waves maintain a constant velocity regardless of the impulse magnitude, and even along a curved path. Our metamaterial could open exciting possibilities for designing nonlinear materials with exotic topological properties.

DOI: [10.1103/PhysRevApplied.18.054049](https://doi.org/10.1103/PhysRevApplied.18.054049)

I. INTRODUCTION

Reciprocity is often assumed for ordinary materials, where wave propagation between two points within a medium is the same in both amplitude and velocity [1–3]. However, metamaterials have been recently shown to achieve nonreciprocity [3–10], typically within certain nonlinear systems. However, nonlinearity does not imply nonreciprocity, and in many systems also utilizes some breaking of symmetry (such as time reversal or spatial symmetry). For example, adding a defect to the edge of a granular chain of nonlinear beads can break spatial symmetry thus introducing nonreciprocity [11,12]. In other cases, symmetry has been broken by engineering bistability on the individual element level [9,13,14] or on an entire structural level [15]. In such bistable metamaterials, unidirectional transition waves can utilize stored potential energy as a means of stabilizing a propagating topological soliton [7,13]. Acoustic metamaterials that break reciprocity have been explored for potential applications such as acoustic wave guides [16,17], acoustic logic elements [7,12,18], and acoustic topological insulators [19–21]. Most of the current designs of nonreciprocal metamaterials confine wave propagation to a fixed single direction, velocity, or single occurrence with no or limited tunability.

II. RECIPROCITY BY DESIGN

In this paper, we present a dynamically tunable, or *reprogrammable*, metamaterial that can support the propagation of unidirectional transition waves in a variety of directions and wave speeds. Our material is composed of free-floating disks with embedded permanent magnets confined in-plane with a programmable magnetic boundary. The boundary is made out of four rows of embedded permanent magnets that can slide past each other (e.g., through an Arduino and a 9-V motor) to change the boundary's magnetic field. The basic building block (i.e., unit cell) is considered as a single disk surrounded by six permanent magnets in the boundary, four within the inner boundary and two within the outer boundary [Fig. 1(a)]. We harness asymmetric bistability to allow the material's unit cells to support the propagation of topological solitons in one direction. Our material can be tuned to change the behavior of the soliton propagation between reciprocal, nonreciprocal, and no propagation within the same metamaterial design. In addition, the direction of the transition wave can be reversed through a simple mechanical adjustment that can easily be programmed [Fig. 1(b)]. Moreover, the released potential energy of the metamaterial can be restored through the same mechanism used for programming its reciprocity.

III. ENERGY LANDSCAPE

We start our analysis by considering the energy landscape within our metamaterial. The potential energy of

*osama.bilal@uconn.edu

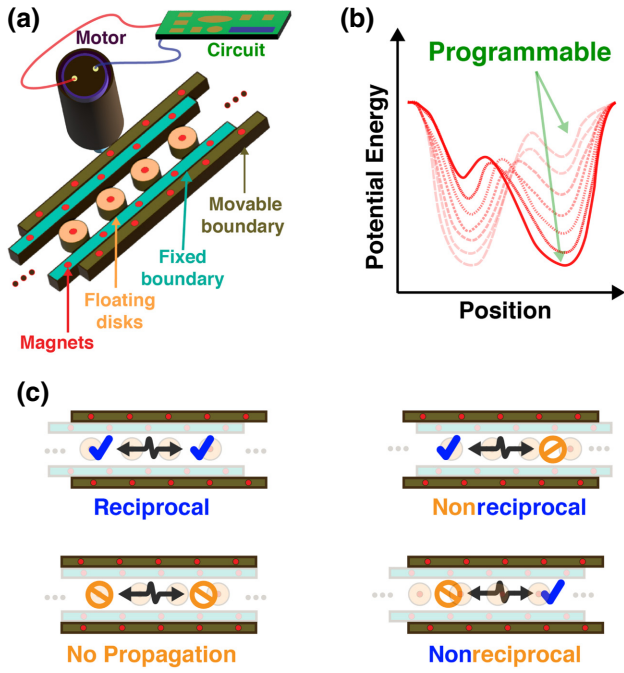


FIG. 1. Concept. (a) Schematic of the proposed metamaterial composed of floated disks surrounded by two magnetic boundaries that can slide against each other by a programmable motor. (b) The programmable potential-energy landscape of the same unit cell with different boundary alignment. (c) The different possibilities for transition waves through the metamaterials.

a given unit cell, of length L [Fig. 2(a)], can be calculated through the integration of the repulsion forces, F , between the disks' and the boundary's magnets as $PE_x = \int_0^L -F_x dx$ [Fig. 2(b)] [22,23]. To identify the nature of the wave-propagation characteristics within a given lattice, we calculate the necessary activation energy, E_a , to move a disk from its stable energy state (its current energy potential well) to the next. In addition, we calculate the amount of released energy due to a potential well switching, E_k . Depending on the balance between the activation and released energy E_a and E_k , a lattice can allow four scenarios for a transition wave to propagate [Fig. 1(c)]: [24] (1) only to the left, (2) only to the right, (3) either left or right, and (4) neither left nor right. To classify each lattice-parameter combination, we find the x position with the lowest potential energy, x_{\min} , which lies either to the left or the right of the inner boundary's magnet position, δ . Propagation in the forward direction occurs if the potential energy of the disk is greater than the required activation energy (E_{a1}), for a value of x between δ and x_{\min} . Wave propagation in the reverse direction occurs if $PE_{\text{disk}} > E_{a2}$ for a value of x between x_{\min} and L .

To explore the design space of our metamaterial, we vary both the boundary separation distance, S , and the relative position of the inner boundary magnets, δ , while keeping the unit-cell dimensions, $L = 40$ mm and $W = 15$ mm,

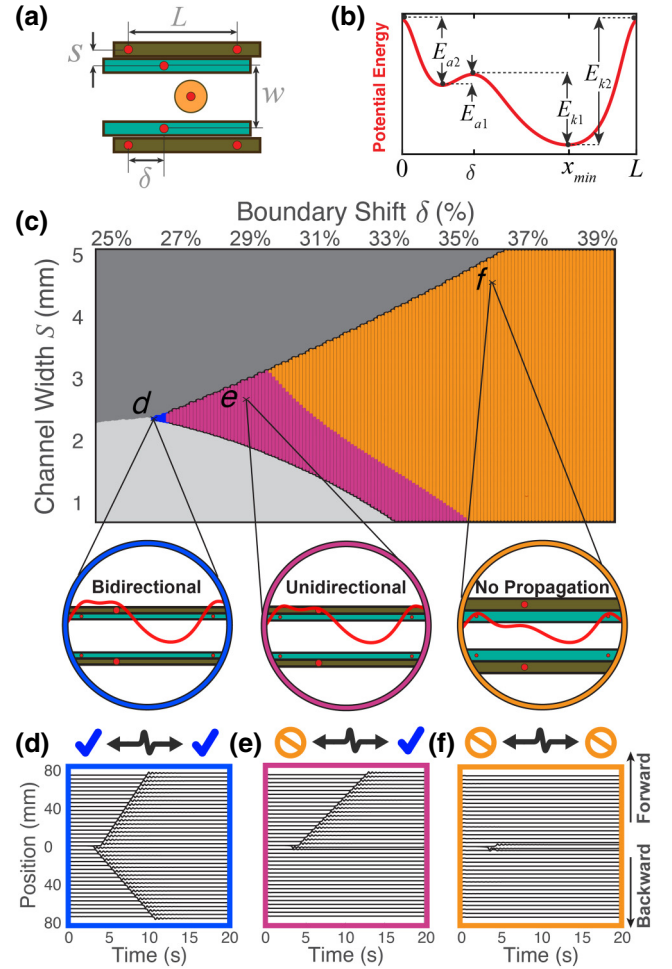


FIG. 2. Potential energy landscape. (a) Schematic of the unit cell. (b) The potential energy landscape of a single unit cell as a function of position. (c) Classification of wave behavior within the metamaterial as a function of δ and S . The inset displays three examples of bistable metamaterials with reciprocal (blue), nonreciprocal (magenta), and no propagation (orange) of transition waves. Outside the bistable region, the monostable regions are highlighted in gray. (d)–(f) Numerically simulated displacement of each metamaterial case as a function of time in both the forward and backward direction.

fixed [Fig. 2(a)]. The varying strength of the magnets, position, and proximity to the disk can give rise to asymmetric bistability in the disk's potential energy landscape. All considered configurations are asymmetric as $\delta \neq L/2$. However, bistability is not guaranteed for all configurations despite the asymmetry. For example, for small δ ($< 26\%$), the potential energy landscape is monostable. Such monostability arises from the close proximity of the inner and outer boundary magnets, leaving no potential well for the disk to rest between 0 and δ [gray shaded regions in Fig. 2(c)]. The direction of the preferred rest position of the disk within a monostable configuration is a function

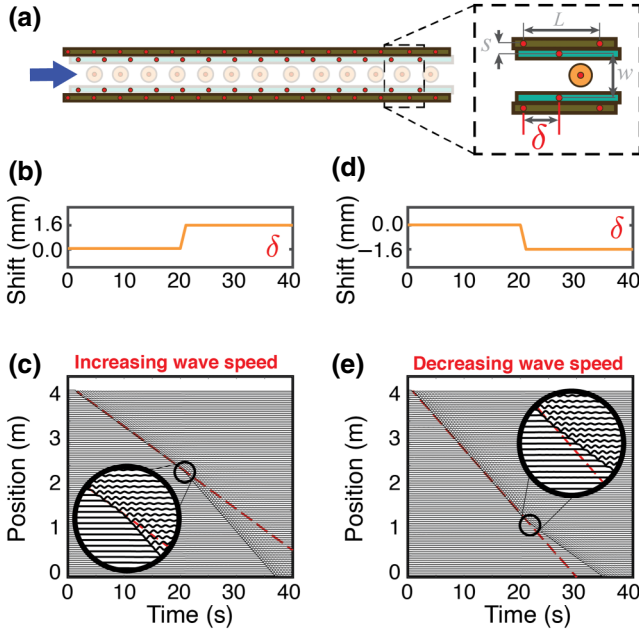


FIG. 3. Wave speed tuning. (a) Schematic of the metamaterial with an inset showing the different parameters of the unit cell. (b),(d) The programmed change of the position of the inner boundary magnets as a function of time. (c),(e) The displacement of each disk as a function of time. The dashed red line shows the original speed of sound in the metamaterial. The inset in (c),(e) shows the onset of the change in the speed of sound.

of the distance between the inner and the outer boundary, S . For lower values of S , the disk slides right, while higher S values cause the disk to slide left instead (see Supplemental Material [25]). Within the configurations that are bistable, all four aforementioned different transition wave scenarios are possible through a simple change in the unit-cell parameters [Fig. 2(c)—insets]: reciprocal (blue), nonreciprocal forward or backward (magenta), and no propagation (orange). More interestingly, for the same design with fixed S , W , and L , a shift in the position of the inner-boundary magnets, δ , spans all four scenarios. In other words, one can program the same metamaterial design with any desired reciprocity or nonreciprocity traits by a 10% relative shift between the boundaries.

IV. NUMERICAL SIMULATION

To verify our analytical predictions about the dynamical characteristics of the different metamaterial designs, we numerically simulate the propagation of the wave within an array of 20 unit cells using the Verlet method [26]. We select three examples within the bistable parameter map for (i) reciprocal propagation in both directions [Fig. 2(d)], (ii) nonreciprocal propagation in one direction only [Fig. 2(e)], and (iii) no propagation of the wave in either direction [Fig. 2(f)]. We apply a relatively small

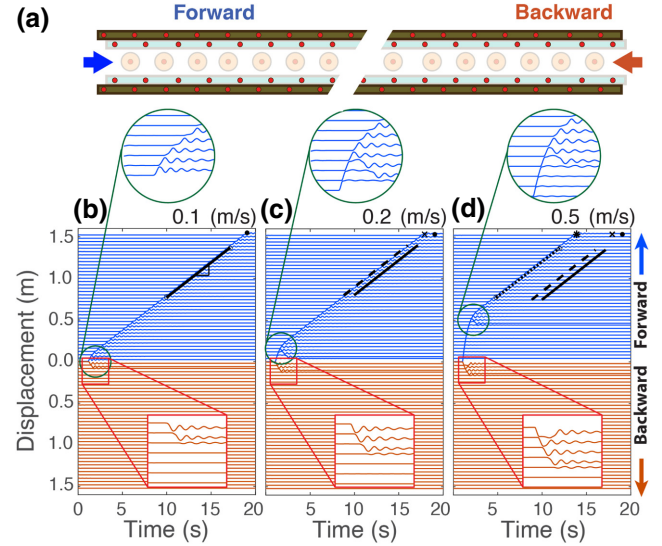


FIG. 4. Nonreciprocity under different loads. (a) Metamaterial schematic with forward and backward excitation. (b)–(d) Displacement of each disk as a function of time for different impulse intensities for both the forward (blue) and backward (orange) directions. The black lines represent the propagating wave velocity for an impulse of 0.1 m/s (solid), 0.2 m/s (dashed), and 0.5 m/s (dotted). The black lines for each lower excitation intensity are kept on for each next panel as a reference.

amount of damping in the simulations to ensure the convergence of the disks to their equilibrium positions (see Supplemental Material [25]). In each of the considered cases (i)–(iii), we apply a load at the rightmost unit cell and record the propagation of the transition wave in the forward (i.e., applied load) direction. In a separate simulation, we apply the same load at the leftmost unit cell and record the propagation of the wave in the backward (i.e., opposite of the original applied load) direction. The nonreciprocal design allows wave propagation in the forward direction only, while the initiated wave in the backward direction immediately dies out [Fig. 2(e)]. The transition wave propagates in neither direction for the metamaterial with expected no propagation. [Fig. 2(f)]. It is worth noting that the wave *velocity* as well as its *penetration depth* varied between the different simulated designs and even between forward and backward propagation for the same design (Fig. 7).

To further explore the variation in the velocity of the propagating wave, we consider a metamaterial array composed of 100 unit cells. We numerically simulate an impulse excitation at the leftmost unit cell of the metamaterial triggering a transition wave moving forward [Fig. 3(a)]. The wave travels at a constant speed of approximately equal to 83.5 mm/s. While the wave is propagating, at $t = 20$ s, we apply a shift to the outer boundary of the metamaterial changing δ for each unit cell by +1.6 mm [Fig. 3(b)]. The shift causes an on-the-fly increase of the

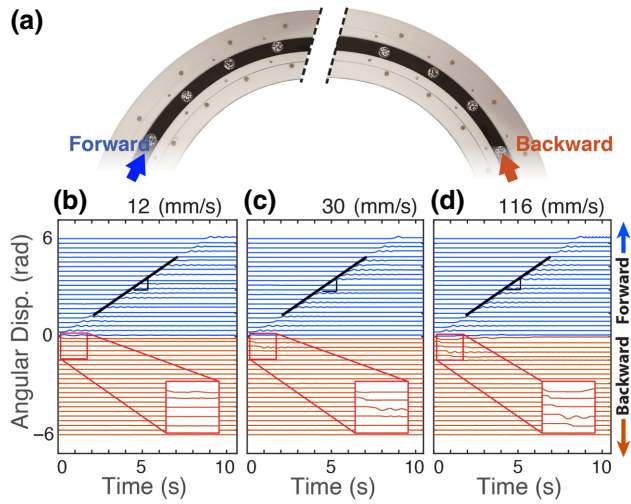


FIG. 5. Experimental excitation with different impulses. (a) Image of a section of the experimental sample. (b)–(d) Displacement of each disk as a function of time for different impulse intensities for both the forward (blue) and backward (orange) directions.

wave velocity as it propagates through the metamaterial [Fig. 3(b)]. The dashed red line in Fig. 3(c) shows the original velocity of the wave. The same tuning parameter is used to slow the speed of the propagating wave by changing δ by -1.6 mm [Fig. 3(e)].

To capture the effect of the impulse amplitude on the velocity and penetration depth of the transition wave, we consider the nonreciprocal configuration of our metamaterial [Fig. 2(e)] under different loading conditions. For different impact velocities, the nonreciprocity of the metamaterial is not altered, i.e., the transition wave can still propagate only in the forward direction [Figs. 4(b)–4(d)]. In the backward direction, however, the number of activated unit cells, or the wave penetration depth, varies depending on the impact velocity (two unit cells for 0.1 m/s, three for 0.2 m/s, and four for 0.5 m/s). In the forward direction, the wave propagates through the entire metamaterial array, but reaches the end at different times [indicated by markers on Figs. 4(b)–4(d)], as the *initial* wave speed varies significantly depending on the intensity of the impulse. However, in every case the wave speed decays eventually reaching a constant speed (i.e., steady state) of approximately equal to 83.5 mm/s [indicated by black lines in Figs. 4(b)–4(d)]. Therefore, we can conclude that the magnitude of impulse does not affect the steady-state wave velocity in the system. It is also worth noting that for higher amplitude impulses, as the wave reaches its steady-state propagation speed, a portion of the wave energy is reflected in the backward direction [Figs. 4(c) and 4(d)]. However, due to nonreciprocity, the energy reflected in the backward direction does not persist.

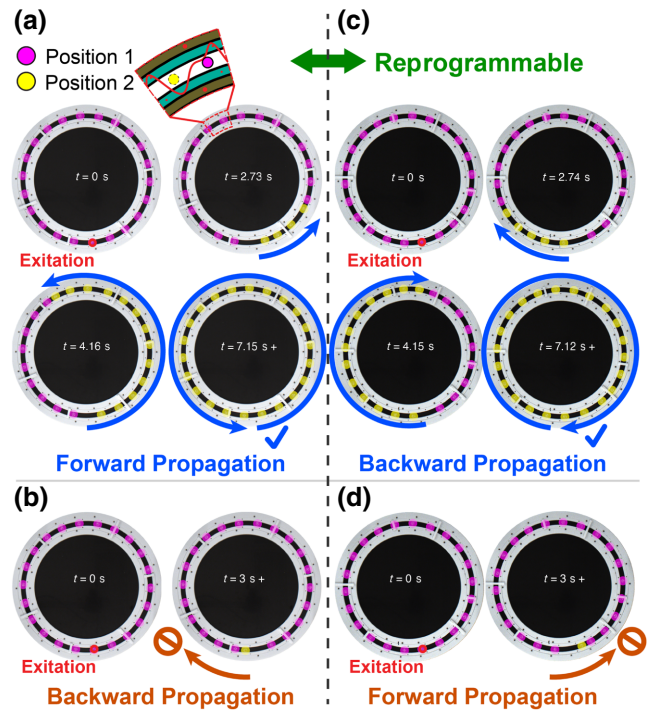


FIG. 6. Reprogramming. (a) Counterclockwise excitation of a wave through the ring when configured for counterclockwise wave propagation. Diagram representing two positions (potential wells), which are labeled in the diagram. (b) Clockwise excitation of a wave through the ring when configured for only counterclockwise wave propagation. (c) Clockwise excitation of a wave through the ring when configured for clockwise wave propagation. (d) Counterclockwise excitation of a wave through the ring when configured for only clockwise wave propagation. The final images in each case show the system after steady state has been reached while the time represents how long it took for the final disk to cross the potential energy barrier.

V. EXPERIMENTAL VALIDATION

After the transition wave propagates, the disk in each unit cell shifts from a high- to a low-energy state, rendering the system a single use only. The same method that we utilize for tuning the metamaterial properties, i.e., shifting the outer boundary, can be used to reset all the unit cells at once. However, for a metamaterial with equal length of inner and outer boundaries, there exist only a finite number of available resets in one direction. In addition, each time a reset takes place, the metamaterial is shortened by one unit cell. In other words, the inner or outer boundaries of the finite system can slide only so far before they become completely separated. To overcome these limitations in an experiment, we design and fabricate a circular boundary for our materials, which is infinitely periodic. Such a metamaterial configuration can be reset an infinite number of times (see Supplemental Videos [25]). We start by testing the implication of the curvature on the nonreciprocal behavior of the metamaterials. We design a

circular metamaterial with 22 unit cells that allows transition waves to propagate only in the clockwise direction. The disks are floated on an air bearing within the x - y plane [27–32] (same as the arcade game, air hockey) to minimize friction [Fig. 5(a)]. We apply an impulse of various intensities in both clockwise (CW) and counterclockwise (CCW) directions using an impactor. We track the disk motion using digital image correlation engine (DICE) software as a function of time [Figs. 5(b)–5(d)]. The wave propagates only in the forward (CCW) direction regardless of the impact velocity. In the backward direction, the wave stops after penetrating at different depths (1–5 unit cells) depending on the impact velocity, validating our analytical and numerical predictions. We further test the validity of our programming of the metamaterial by first aligning its boundaries to allow the wave to propagate in the CCW direction [Fig. 6(a)], but not the CW direction [Fig. 6(b)]. Then, we shift the outer boundary of the metamaterial to set the CW direction into the new direction of propagation [Fig. 6(c)]. This in turn prevents the wave from propagating CCW [Fig. 6(d)]. Both CW and CCW propagating waves have the same propagating velocity (arrive within ∓ 0.015 s of each other).

VI. CONCLUSION

We study analytically, numerically, and experimentally a metamaterial with reprogrammable wave-propagation characteristics. Our metamaterial is composed of a lattice of repelling magnetic disks confined within a magnetic boundary. Depending on the surrounding magnetic field, the system can be either reciprocal or nonreciprocal, allowing transition waves to propagate in both directions, in one direction, or in neither direction. We validate our system’s performance under different loading conditions. We numerically observe two different wave velocities, transient, and steady state, for a propagating transition wave as a function of the applied load. In addition, we can program the magnetic field to significantly increase or decrease the velocity of the propagating wave. Due to the simplicity of the system, a programmable shift or slide within the boundary can cause the system to change wave-propagation velocity, direction or both. Moreover, the shift in the boundary can be used to recharge or reset the entire system all at once. Our findings can prove useful in designing nonlinear materials with exotic topological properties that can be tuned in real time, opening the door for advanced functional devices.

APPENDIX A: ANALYTICAL MODEL

The repulsive force between two magnetic dipoles can be written as [22,23] $\vec{F}_{ij} = \mu_0/4\pi \vec{\nabla} \cdot [\vec{m}_i \cdot \vec{m}_j/r^3 - 3(\vec{m}_i \cdot \vec{r}) \cdot (\vec{m}_j \cdot \vec{r})/r^5]$, where μ_0 is the permeability of the medium, \vec{m}_i and \vec{m}_j are the magnetic moments between

magnets i and j , and \vec{r} is the separation vector between the magnets. Because \vec{m}_i and \vec{r} are orthogonal in our design [27–30] and \vec{m}_i and \vec{m}_j are parallel, the equation can be rewritten as $\vec{F}_{ij} = 3\mu_0 m_i m_j / 4\pi r^4 = Ar^{-4}$. We consider a nearest-neighbor interaction model between the unit cells. The equation of motion of disk n along the x direction, x_n can be written as

$$M\ddot{x}_n = \sum_{i=0}^2 A_1 \frac{D_{ni}}{|D_{ni}|} \left(D_{ni}^2 + \frac{w^2}{4} \right)^{\alpha/2} + \sum_{j=0}^2 A_1 \frac{D_{nj}}{|D_{nj}|} D_{nj}^{\beta} + \sum_{k=0}^2 A_2 \frac{D_{nk}}{|D_{nk}|} \times \left(D_{nk}^2 + \frac{(w+S)^2}{4} \right)^{\beta/2}, \quad (\text{A1})$$

where $D_{n(\cdot)} = (x_n - x_{(\cdot)})$ is the relative distance between disk n and magnet (\cdot) , A_1 and A_2 are the coefficients of repulsive force between magnets pairs, 1.0935×10^{-12} and 9.6170×10^{-10} , respectively. The values $\alpha = -4$, and $\beta = -3.036$ correspond to the experimentally measured exponential coefficient of $F(r)$ with a separation distance r . The length of the unit cell L , is defined as the distance between the corner magnets along the x direction. The width of the unit cell w , is the distance between the inner-boundary magnets directly across the channel.

APPENDIX B: VARIABLE PROPAGATING VELOCITY

Our metamaterial can be designed to have large direction-dependant variations within the wave-propagation velocities. For example, we design a metamaterial that supports the propagation of topological solitons both in the forward and reverse directions. However, the transition wave travels at half the speed in the reverse versus the forward direction. The unit cell length is $L = 42$ mm with a channel width of $w = 15$ mm. The separation distance between the boundary magnets is $S = 2.63$ mm and a shift of $\delta = 29\%L$ (Fig. 7). The damping coefficient used in the simulation is (10^{-3} N s/m). The potential energy landscape of the unit cell shows high asymmetry [Fig. 7(b)]. However, such asymmetry is not the only requirement for the wave to propagate in one direction but not the other, as we demonstrate in the paper’s main text. We simulate an impulse load in the forward direction, and in a separate simulation we apply the *same* load in the reverse direction. We plot the displacement of each disk as a function of time [Fig. 7(c)]. The speed of the wave in the reverse direction is roughly half that of the forward. It is worth noting that the disks oscillate in their potential wells at the same frequency, but in the reverse direction, the neighboring disk does not change potential wells until the second oscillation; where in the forward direction the excitation of

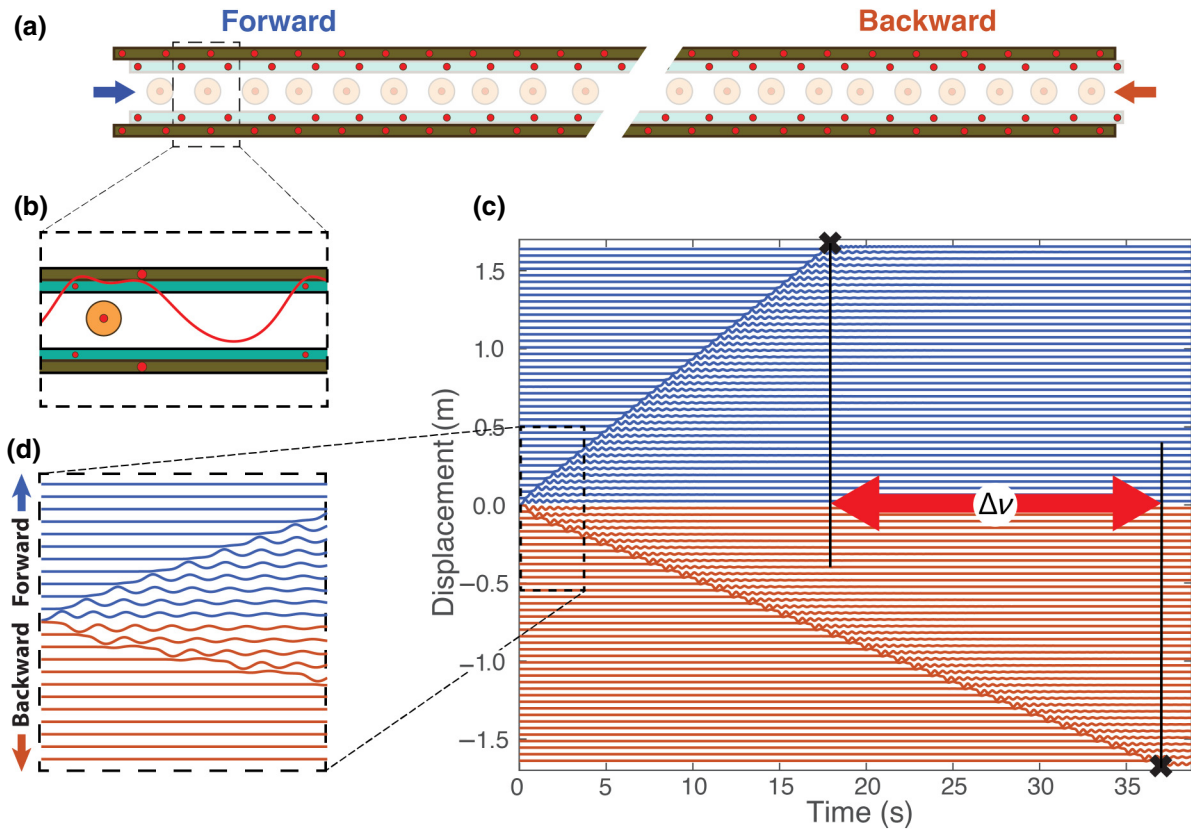


FIG. 7. (a) Metamaterial schematic with forward and backward excitation. (b) The potential energy of a single unit cell as a function of position. (c) Displacement of each disk as a function of time for both the forward (blue) and backward (orange) directions. The black vertical lines represent the time where the wave reaches the end of the lattice. The difference in speed Δv is highlighted by the red arrow. (d) An enlarged view for the first few seconds in the simulation of the propagating wave in both the forward and backward directions.

the neighboring unit cell occurs immediately after the first oscillation [Fig. 7(c)]. The parameters of the unit cell can also be tuned or modified for a different desired behavior depending on the application.

APPENDIX C: EXPERIMENTAL METHODS

The unit cells are composed of a free floating disk with an embedded cylindrical permanent magnet (diameter, $d = 2$ mm and height, $h = 1$ mm) surrounded by six cylindrical permanent magnets in the boundary, four within the inner boundary ($d = 2$ and $h = 1$ mm) and two within the outer boundary ($d = 3$ and $h = 3$ mm). All magnets are aligned in the same orientation acting as monopoles in the x - y plane. The repulsion force between two 2-mm magnets is $\vec{F} = 1.09 \times 10^{-12} \times r^{-4}$ and between the 2- and 3-mm magnets is $\vec{F} = 9.61 \times 10^{-10} \times r^{-3.036}$, where r is the separation distance between the magnets. The propagation of the transition waves is simulated numerically using the Verlet method [26]. The damping coefficient used in the simulations is (10^{-3} N s/m) . The metamaterial is fabricated out of a 3-mm-thick acrylic sheet. The disks

are floated on an air bearing (New way S1030002). The fabricated circular boundary is composed of four concentric rings of embedded magnets with diameters 224, 235.3, 268.6, and 280 mm. The disk mass is 0.118 g. The tracking is done through a computer vision camera (Blackfly S USB3) and the captured images are analyzed using DICe. The disks and boundaries of the metamaterials are fabricated using a laser cutter (Spectrum Pro-series 24). All the embedded permanent magnetic dipoles are oriented in the same direction (i.e., north-seeking pole pointing up) causing the disk magnets as well as boundary magnets to act as monopoles in two dimensions. Both the inner boundary and disks in the system use the 2 by 1 mm (diameter and height, respectively) magnets whose centroids are all in plane with one another. The outer ring uses a 3 by 3 mm magnet whose centroid is raised slightly higher than that of the other magnets due to its larger height [Fig. 8(b)]. We assume a repulsive force with negligible difference from what would be found if all magnets were perfectly in plane. The disks are floated on top of an air bearing to reduce friction. To ensure a minimal amount of friction, we attach a glass slide at the bottom of each disk [27,31,32]. For

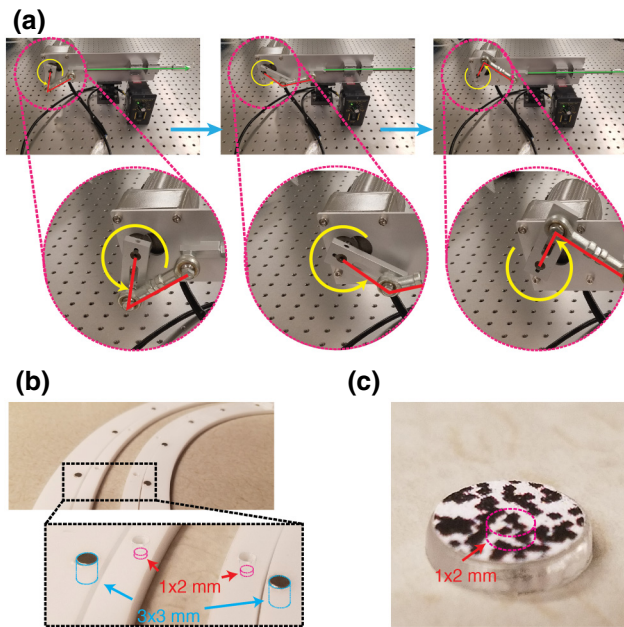


FIG. 8. Images showing various components of the experimental setup. (a) The linear actuator motion is shown as a motor driven arm extends and retracts with enlarged insets. (b) The circular boundary with the magnets embedded within. (c) A single disk decorated with a speckle pattern for better digital image correlation tracking. The embedded magnet within is outlined by superimposed dotted lines.

impulse excitation, we utilize a reciprocating linear actuator (BEMONOC) driven by an electric motor at a constant rotational speed [Fig. 8(a)]. The rotation driven arm has a sinusoidal velocity, with the reported velocity in Figs. 5(b)–5(d) being the recorded velocity at the time of the impact with the excited disk. The floated disks are tracked using the DICe. To help DICe track the disks, we place a circular-shaped paper with a unique speckle pattern at the top of each disk [Fig. 8(c)].

- [1] Horace Lamb, On reciprocal theorems in dynamics, *Proc. London Math. Soc.* **1**, 144 (1887).
- [2] Michael B. Muhlestein, Caleb F. Sieck, Andrea Alù, and Michael R. Haberman, Reciprocity, passivity and causality in Willis materials, *Proc. R. Soc. A: Math., Phys. Eng. Sci.* **472**, 20160604 (2016).
- [3] Romain Fleury, Dimitrios L. Sounas, Caleb F. Sieck, Michael R. Haberman, and Andrea Alù, Sound isolation and giant linear nonreciprocity in a compact acoustic circulator, *Science* **343**, 516 (2014).
- [4] Giuseppe Trainiti, Yiwei Xia, Jacopo Marconi, Gabriele Cazzulani, Alper Erturk, and Massimo Ruzzene, Time-Periodic Stiffness Modulation in Elastic Metamaterials for Selective Wave Filtering: Theory and Experiment, *Phys. Rev. Lett.* **122**, 124301 (2019).
- [5] Lisa M. Nash, Dustin Kleckner, Alismari Read, Vincenzo Vitelli, Ari M. Turner, and William T. M. Irvine, Topological mechanics of gyroscopic metamaterials, *Proc. Nat. Acad. Sci.* **112**, 14495 (2015).
- [6] Yangyang Chen, Xiaopeng Li, Hussein Nassar, Andrew N. Norris, Chiara Daraio, and Guoliang Huang, Nonreciprocal Wave Propagation in a Continuum-Based Metamaterial with Space-Time Modulated Resonators, *Phys. Rev. Appl.* **11**, 064052 (2019).
- [7] Jordan R. Raney, Neel Nadkarni, Chiara Daraio, Dennis M. Kochmann, Jennifer A. Lewis, and Katia Bertoldi, Stable propagation of mechanical signals in soft media using stored elastic energy, *Proc. Nat. Acad. Sci.* **113**, 9722 (2016).
- [8] Noah Kruss and Jayson Paulose, Nondispersive One-Way Signal Amplification in Sonic Metamaterials, *Phys. Rev. Appl.* **17**, 024020 (2022).
- [9] H. Yasuda, L. M. Korpas, and J. R. Raney, Transition Waves and Formation of Domain Walls in Multistable Mechanical Metamaterials, *Phys. Rev. Appl.* **13**, 054067 (2020).
- [10] Hussein Nassar, Behrooz Yousefzadeh, Romain Fleury, Massimo Ruzzene, Andrea Alù, Chiara Daraio, Andrew N. Norris, Guoliang Huang, and Michael R. Haberman, Nonreciprocity in acoustic and elastic materials, *Nat. Rev. Mater.* **5**, 667 (2020).
- [11] Neil Boechler, Georgios Theocharis, and C. Daraio, Bifurcation-based acoustic switching and rectification, *Nat. Mater.* **10**, 665 (2011).
- [12] Feng Li, Paul Anzel, Jinkyu Yang, Panayotis G. Kevrekidis, and Chiara Daraio, Granular acoustic switches and logic elements, *Nat. Commun.* **5**, 1 (2014).
- [13] Neel Nadkarni, Andres F. Arrieta, Christopher Chong, Dennis M. Kochmann, and Chiara Daraio, Unidirectional Transition Waves in Bistable Lattices, *Phys. Rev. Lett.* **116**, 244501 (2016).
- [14] Bolei Deng, Pai Wang, Vincent Tournat, and Katia Bertoldi, Nonlinear transition waves in free-standing bistable chains, *J. Mech. Phys. Solids* **136**, 103661 (2020).
- [15] Gabriele Librandi, Eleonora Tubaldi, and Katia Bertoldi, Programming nonreciprocity and reversibility in multistable mechanical metamaterials, *Nat. Commun.* **12**, 1 (2021).
- [16] Romain Fleury, Alexander B. Khanikaev, and Andrea Alu, Floquet topological insulators for sound, *Nat. Commun.* **7**, 1 (2016).
- [17] Thibaut Devaux, Vincent Tournat, Olivier Richoux, and Vincent Pagneux, Asymmetric Acoustic Propagation of Wave Packets via the Self-Demodulation Effect, *Phys. Rev. Lett.* **115**, 234301 (2015).
- [18] A. A. Maznev, A. G. Every, and O. B. Wright, Reciprocity in reflection and transmission: What is a ‘phonon diode’?, *Wave Motion* **50**, 776 (2013).
- [19] Roman Süssstrunk and Sebastian D. Huber, Observation of phononic helical edge states in a mechanical topological insulator, *Science* **349**, 47 (2015).
- [20] Pai Wang, Ling Lu, and Katia Bertoldi, Topological Phononic Crystals with One-Way Elastic Edge Waves, *Phys. Rev. Lett.* **115**, 104302 (2015).
- [21] Noah P. Mitchell, Lisa M. Nash, Daniel Hexner, Ari M. Turner, and William Irvine, Amorphous topological insulators constructed from random point sets, *Nat. Phys.* **14**, 380 (2018).

- [22] Ahmed Mehrem, Noe Jimenez, L. J. Salmerón-Contreras, X. García-Andrés, L. M. García-Raffi, R. Picó, and Víctor José Sánchez-Morcillo, Nonlinear dispersive waves in repulsive lattices, *Phys. Rev. E* **96**, 012208 (2017).
- [23] David J. Griffiths, Introduction to electrodynamics, (2005).
- [24] The energy lost to damping does not deteriorate the transition wave. if the release of energy from one unit cell is enough to trigger the release in the neighboring unit cell, new energy released from the neighbor will be enough to continue the wave.
- [25] See Supplemental Material at <http://link.aps.org/supplemental/10.1103/PhysRevApplied.18.054049> for more details on the numerical and experimental methods.
- [26] William H. Press, Saul A. Teukolsky, William T. Vetterling, and Brian P. Flannery, *Numerical Recipes 3rd Edition: The art of Scientific Computing* (Cambridge university press, New York, New York, 2007).
- [27] Audrey A. Watkins and Osama R. Bilal, Demultiplexing infrasound phonons with tunable magnetic lattices, *Front. Mater.* **7**, 410 (2020).
- [28] Ehsan Norouzi, Audrey A. Watkins, and Osama R. Bilal, Classification of emerging patterns in self-assembled two-dimensional magnetic lattices, *Phys. Rev. E* **104**, 044902 (2021).
- [29] Audrey A. Watkins, Austin Eichelberg, and Osama R. Bilal, Exploiting localized transition waves to tune sound propagation in soft materials, *Phys. Rev. B* **104**, L140101 (2021).
- [30] Audrey A. Watkins, Austin Eichelberg, and Osama R. Bilal, Harnessing Reprogrammable Phase Transitions to Control the Propagation of Sound Waves, *Phys. Rev. Appl.* **17**, 024036 (2022).
- [31] Miguel Molerón, Christopher Chong, Alejandro J. Martínez, Mason A. Porter, Panagiotis G. Kevrekidis, and Chiara Daraio, Nonlinear excitations in magnetic lattices with long-range interactions, *New J. Phys.* **21**, 063032 (2019).
- [32] Marc Serra-Garcia, Miguel Molerón, and Chiara Daraio, Tunable, synchronized frequency down-conversion in magnetic lattices with defects, *Philos. Trans. R. Soc. A: Math., Phys. Eng. Sci.* **376**, 20170137 (2018).